E-proceedings of the 38th IAHR World Congress
September 1-6, 2019, Panama City, Panama
doi:10.3850/38WC092019-0211

HYDRAULICS OF AN ASYMMETRICAL FLUME WITH SIDEWALL RIB TO ASSIST WITH FISH PASSAGE

PEDRO SANCHEZ[(1)], XINQIAN LENG[(2)] & HUBERT CHANSON[(3)]

[(1,2,3)] The University of Queensland, School of Civil Engneering, Brisbane QLD 4072, Australia
e-mail h.chanson@uq.edu.au

ABSTRACT

Channels with streamwise ribs have been studied for decades in chemical engineering, environmental and sanitary engineering, aeronautics, astronautics, biology and geology. Recently a biological study suggested that lateral longitudinal beam might assist with the upstream passage of small-bodied fish in hydraulic structures. Herein a detailed hydrodynamic study was conducted in an asymmetrical rectangular channel equipped with a sidewall square (50mm×50mm) rib in a culvert barrel channel. Both free-surface, velocity and boundary shear stress measurements showed strong secondary currents of Prandtl's second kind. The sidewall rib and channel asymmetry contributed to intense secondary motion, associated with turbulent dissipation. The channel design provided a small well-defined highly-turbulent low-velocity zone (LVZ) beneath the rib. In the context of hydraulic structure designs, uttermost care must be considered because of manufacturing, installation and operational issues. In many instances, alternative designs should be preferred to assist with fish passage in hydraulic structures. Altogether this detailed investigation demonstrated how the introduction of a seemingly simple streamwise shape, i.e. a sidewall square rib, may induce a major change in hydrodynamic properties, in comparison to a simple rectangular channel flow.

Keywords: Open channel hydrodynamics, Sidewall longitudinal rib, Secondary flows, Physical modelling, Sedimentation.

1 INTRODUCTION

While the literature on transverse beams is very extensive in mechanical, aeronautical, chemical, civil and environmental engineering (Morris 1955, Knight and Macdonald 1979), channels with longitudinal beams have also been studied for decades and the idea is not novel. Streamwise beams along channel walls have been successfully tested for the increased heat transfer rate (Naik et al. 1999, Chang et al. 2008) and mass transfer in chemical engineering (Stamou 2008). A related design was developed for biological filtration (Roo 1965). Longitudinal beams are used in a number of stages of water treatment plants, e.g. maze flocculator, high-rate clarification tube settler, sedimentation basin with plate settlers, sludge clarifier (Degremont 1979, Randtke and Horsley 2012). Similar designs are also used on stormwater treatment systems and combined sewers (FNDAE 1988). In alluvial channels, long-lasting three-dimensional large-scale turbulent vortices may yield the development of longitudinal troughs and ridges on the mobile bed with preferential transport of bed particles along troughs (Nezu and Nakagawa 1984). Longitudinal ridges and runnels were also reported in intertidal zones (Carling et al. 2009). Related observations include massive scour features, with longitudinal ridges and grooves, and streamlined bar forms, in debris flows on Planet Mars (Tanaka 1999).

Small-scale streamwise ribs, also called V-groove riblets, can produce consistent net drag reduction, when the appropriate groove spacing yields a reduction in viscous drag by displacing longitudinal vortices away from the wetted surface, thus reducing their intensity (Bushnell and McGinley 1989). The scales of fast swimming sharks have fine longitudinal ridges, comparable to longitudinal grooves and riblets, that reduce the flow resistance of a surface, enabling drag reduction and faster fish swimming (Nitschke 1983). A related application is the flow past seal fur, achieving drag reductions of up to 12%, due to the streamwise fur pattern (Itoh et al. 2006).

Recent biological tests suggested that a streamwise rib might facilitate the upstream passage of small body-mass fish species. The aim of the present hydraulic investigation is to characterise the role of longitudinal rib on the turbulent flow field in a rectangular channel, corresponding to a standard box culvert

barrel (Fig. 1), and to gain some fundamental understanding of the implications in terms of upstream fish passage. Engineering design considerations are then discussed.

Figure 1. Outlet of multicell box culvert along Witton Creek (Indooroopilly QLD, Australia) on 18 March 2019 after a storm. Flow direction from left to right.

2 PHYSICAL FACILITIES AND INSTRUMENTATION

2.1 Experimental facility

The physical investigation was conducted in the Hydraulics Laboratory of the Advanced Engineering Building at the University of Queensland, in a 15 m long 0.5 m wide (B = 0.50 m) horizontal flume. The bed and sidewalls of the flume were made of PVC and glass respectively (Fig. 2). Upstream of the flume, the water was supplied by a 2.0 m long 1.25 m wide intake structure, fed by a constant head tank, and equipped with baffles, flow straighteners and a three-dimensional convergent leading to the 15 m long flume. The intake structure design allowed smooth inflow conditions at the flume's upstream end. At the downstream end, the flume ended with a free overfall.

A 12 m long 50mm×50mm square rib was installed along the right sidewall. The rib was made out of acrylic sheets cut with an industrial saw, based upon the dimensions of Watson et al. (2018). The square profile had sharp edges and was installed at Z_R = 0.050 m above the bed with an accuracy of ±1 mm over its full length. The longitudinal rib was located between x = 1 m and 13 m, where x is the longitudinal distance from the inlet of the flume and positive downstream. Photographic information on the experimental facility is presented in Sanchez et al. (2018), together with further construction details.

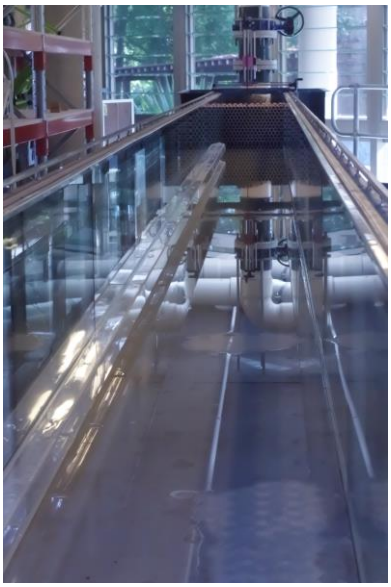

(a)

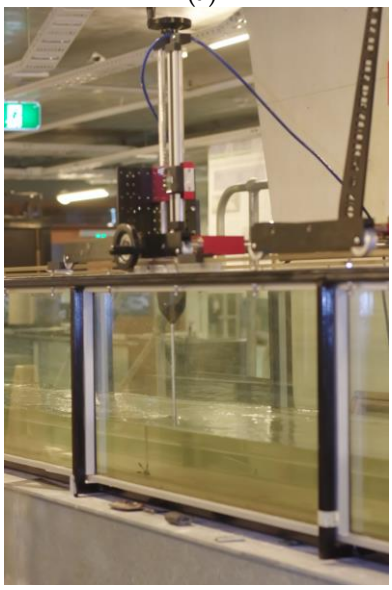

(b)

(c)

Figure 2. Physical model of box culvert barrel with an asymmetrical rib (50mm×50mm) along the right sidewall. (a) Looking upstream at the dry channel with the intake structure in the background. (b) Channel operation for Q = 0.0556 m^3/s with an ADV in position, flow direction from right to left. (c) Detail of the roving Preston tube type C1.6(r) with its measurement tapping below the asymmetrical rib for Q = 0.0556 m^3/s with the flow direction from left to right.

2.2 Instrumentation

The water discharge was measured using a Venturi meter installed in the water supply line and designed according to British standards. The percentage of error of the flow rate was estimated to be less than 2%. A rail-mounted pointer gauge was used to measure the free surface elevation with an accuracy of ±0.5 mm. Three velocimeter systems were used: a Prandtl-Pitot tube, a roving Preston tube (RPT) and an acoustic Doppler velocimeter (ADV). A Dwyer® 166 Series Prandtl-Pitot tube with a 3.18 mm outside diameter (OD) tube was used to measure the velocity and pressure in the water flow. Further velocity measurements were performed with a roving Preston tube (RPT) type C1.6(r) (Fig. 2c). The RPT comprised two stainless steel pressure tubes: a dynamic pressure tube (1.62 mm OD) with 20 mm upstream projection; and a wake pressure tube (1.62 mm OD) directed normal to the boundary surface with a 1 mm clearance (Macintosh 1990) (Fig. 3). The RPT was especially used to measure the velocity field beneath the rib. The Prandtl-Pitot tube and RPT provided two readings: the dynamic pressure in the form of the total head $H^{(1)}$ and the piezometric head $H^{(2)}$ (Fig. 3). The local time-averaged longitudinal velocity component V_x was estimated as:

$$V_x = \frac{1}{\lambda} \times \sqrt{2 \times g \times (H^{(1)} - H^{(2)})} \quad [1]$$

where g = 9.794 m/s^2 in Brisbane and λ = 1.0 and 1.2 for the Prandtl-Pitot tube and RPT respectively, based upon a detailed calibration undertaken on the channel centreline by comparing systematically the vertical distribution of longitudinal velocity (Sanchez et al. 2018).

Additional velocity measurements were performed with an ADV Nortek™ Vectrino+ equipped with a three-dimensional side-looking head. The ADV data were collected, setting a sampling rate of 200 Hz for 180 s at each point. The velocity range was ±1 m/s, the transmit length was 0.3 mm and the control volume was 1 mm. The ADV signal data were post-processed by removing and replacing erroneous data with an average correlation of less than 60% and an average SNR less than 5dB were removed. In addition, the signal was "despiked" using a phase-space thresholding technique (Goring and Nikora 2002, Chanson et al. 2008). During the processing of the data, a rotation angle around the z-axis was applied such that V_y = 0 m/s at the centreline of the channel. For a symmetrical channel, basic considerations shows that the time-averaged transverse velocity component V_y must be zero at all elevations on the centreline of the channel. Although this condition was not strictly correct in the asymmetrical rectangular channel, it enabled a finer adjustment than any other form of manual or mechanical correction of the ADV orientation.

The Prandtl-Pitot tube and RPT may be used to determine the shear stress at a boundary, i.e. the skin friction, in a turbulent channel flow, when the tube is in contact with the wall (Patel 1965, Macintosh 1990, Chanson 2000). Based upon dimensional and theoretical considerations, the boundary shear stress data followed closely an analytical solution of the Prandt mixing length theory for turbulent boundary layer (Cabonce et al. 2017, 2019):

$$(\tau_o)_{skin} = \eta \times \rho \times \kappa^2 \times \frac{V_b^{\ 2}}{N^2} \quad [2]$$

where V_b is the velocity measured by the Prandtl-Pitot or RPT tube lying on the boundary, κ is the von Karman constant: κ = 0.4, N = 7 for a smooth turbulent boundary layer, η = 1 for the Prandtl-Pitot tube and η = 1 to 1.3 for the RPT depending upon the flow conditions and the wake motion behind the dynamic pressure tube (Sanchez et al. 2018).

The vertical translation of the velocity probes was controlled by a fine adjustment travelling mechanism connected to a digital scale unit. The error on the vertical position of the probes was $\Delta z < \pm 0.025$ mm. The accuracy on the longitudinal position was estimated as $\Delta x < \pm 2$ mm. The accuracy on the transverse position of the probe was ±1 mm.

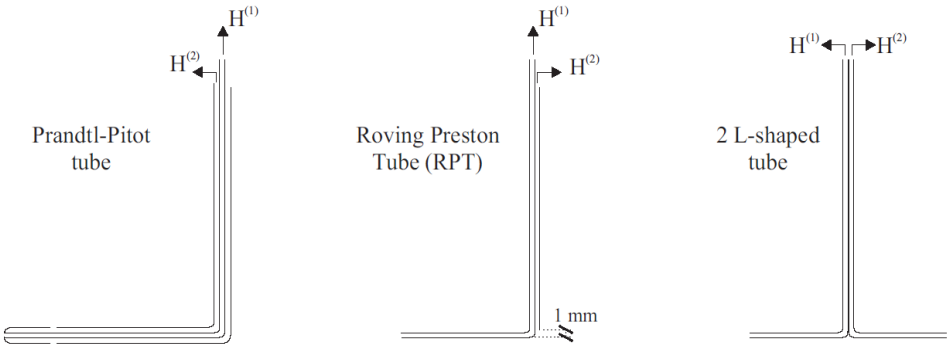

Figure 3. Definition sketches of Prandtl-Pitot tube, roving Preston tube (Type C1.6(c)) and double L-shaped tube system.

2.3 Experimental flow conditions

The experiments were performed for flow conditions corresponding to less-than-design flow conditions in a 1:1 box culvert barrel cell beneath a two-lane road embankment, or a 1:2 scale model of a single cell for the medium-size culvert structure seen in Figure 1. Visual observations and free-surface measurements were conducted for a range of flow rates 0.008 m^3/s < Q < 0.100 m^3/s. Detailed velocity measurements were undertaken for Q = 0.0261 m^3/s, 0.0556 m^3/s and 0.100 m^3/s. Measurements were repeated at different longitudinal locations (x = 1.9 m, 8 m and 11.9 m) and several transversal locations y, where y is the transversal distance from the right sidewall, positive towards the left sidewall. Each vertical velocity profile

consisted of a minimum of 25 points. In addition, boundary shear stress measurements were conducted at each longitudinal location along the entire wetted perimeter, using the Prandtl-Pitot tube and RPT lying onto the bed and walls of the channel, including the rib boundaries.

3 BASIC FLOW PATTERNS

Flow visualisations were conducted for a range of flow rates 0.008 $m^3/s < Q < 0.100$ m^3/s, corresponding to a subcritical flow motion, with decreasing water levels with increasing longitudinal coordinate (H2 backwater profile) (Fig. 4). The water depth was larger than the critical flow depth at all locations along the ribbed channel. Since the channel was asymmetrical, the critical depth must be derived from the minimisation of the specific energy for $Q^2/(g \times A^3/b) = 1$ where Q is the discharge, A is the cross-sectional area, and b is the free-surface width (Henderson 1966, Chanson 2004). The full derivation is presented in Sanchez et al. (2018). The flow patterns observations suggested four flow regimes: (a) Regime I for $d < Z_R$, (b) Regime II for $Z_R < d < (Z_R+h_R)$, (c) Regime III for $d >= (Z_R+h_R)$; and (d) Regime IV for $d >> (Z_R+h_R)$, with d the water depth, Z_R the rib bottom elevation above the channel bed, and h_R the rib height.

Flow regime I was simply a gradually-varied flow (GVF) in a rectangular symmetrical channel and the longitudinal rib had no effect on the flow, observed for $Q < 0.012$ m^3/s. Flow regime II was recorded for 0.012 $m^3/s \leq Q < 0.035$ m^3/s. The sidewall rib interacted with the upper flow region and the free-surface width was narrower: $b = B - l_R$. For $Q \geq 0.035$ m^3/s (Regime III), the free-surface interacted with the upper face of the rib next to the right sidewall. The fluid flow above the rib was affected by some boundary friction and corner flows, forming a low velocity region. Overall the rib tended to shift the main flow, including high-velocity zones, towards the left sidewall. At larger discharges, i.e. $Q >> 0.035$ m^3/s (Regime IV), the main flow was little affected by the sidewall rib, although the fluid flow in the square cavity beneath the right sidewall rib was slower than the main flow.

In Regimes II, III and IV, visual observations and dye injection suggested that the fluid motion in the square cavity beneath the rib tended to be dominated by a secondary motion with an elongated longitudinal large-scale eddy. Dye injection hinted limited mixing between the cavity flow and main flow (Fig. 5).

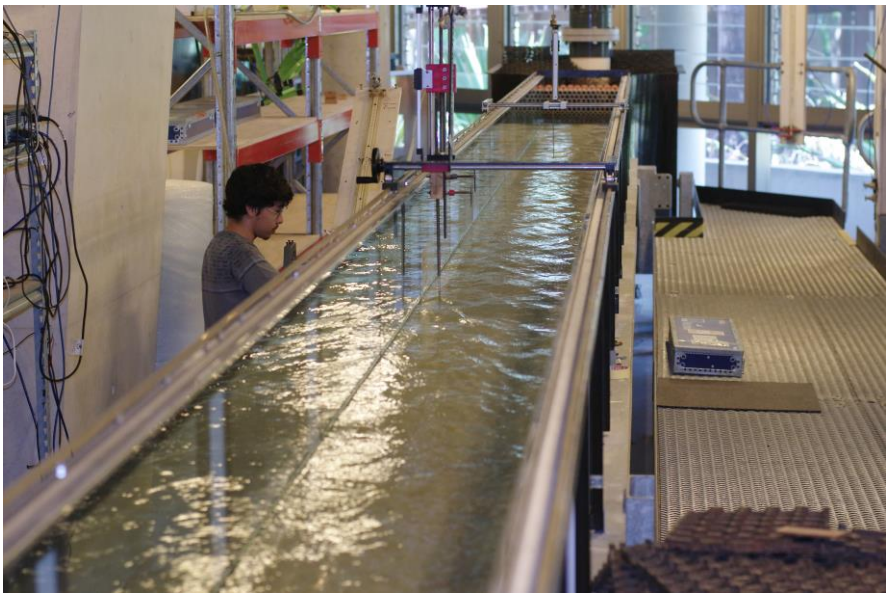

Figure 4. Free-surface flow looking upstream for Q = 0.0.0556 m^3/s. Note the roving Preston tube (RPT) measurements beneath the sidewall rib (also Fig. 2c) and the intake structure in the background. Flow direction from background to foreground.

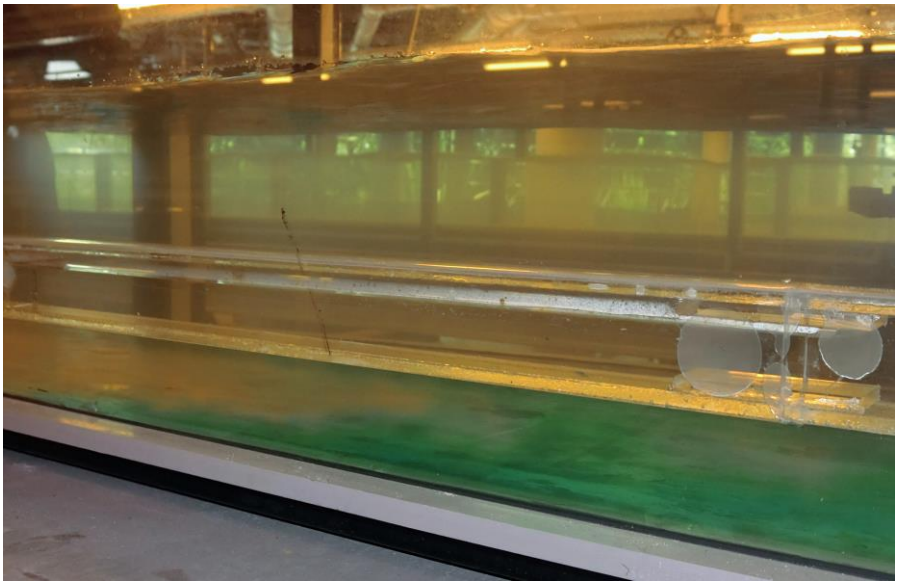

Figure 5. Experiments of dye injection beneath the longitudinal rib for Q = 0.100 m^3/s at x = 8 m. Sideview through the right sidewall, with the flow direction from left to right and the dye injection location beneath the rib.

The flow resistance of the ribbed channel was deduced from free-surface profile measurements and the slope of the total head line. The results are presented in terms of the Darcy-Weisbach friction factor (Table 1). Basically the flow resistance in the ribbed channel was greater than that in a smooth rectangular channel for the same flow conditions. For example, the friction factor of the ribbed channel was nearly twice that for a smooth turbulent flow with a Reynolds number of 50,000. The increased flow resistance was likely caused by strong secondary current motion and intense turbulence induced by the rib presence. The associated turbulent dissipation contributed to both total head losses and flow resistance.

Table 1. Darcy-Weisbach friction factor f of rectangular channel with sidewall square rib (Present study)

Q (m^3/s)	Flow Regime	d at x = 8 m (m)	Re at x = 8 m	f
0.008	I	0.0495	4.89×10^4	0.0405
0.015	II	0.069	8.64×10^4	0.0318
0.0261	II	0.0925	1.41×10^5	0.0248
0.035	III	0.1115	1.69×10^5	0.0230
0.0556	III-IV	0.1475	2.46×10^5	0.0205
0.100	IV	0.2075	3.94×10^5	0.0148

4 VELOCITY AND BOUNDARY SHEAR STRESS MEASUREMENTS

Detailed velocity measurements were conducted in the ribbed channel section, using a combination of velocimeters. In the presence of the sidewall rib, all the longitudinal velocity data showed a consistent pattern. For z > 0.1 m, large velocities were observed about the centreline of the flume. At lower vertical elevations, the maximum longitudinal velocities tended to shift away from the ribbed sidewall towards 0.5 < y/B < 0.7, where B is the internal channel width (B = 0.5 m). A similar pattern was reported by Cabonce et al. (2017,2019) for small triangular baffles installed in the left corner and by Wang et al. (2018) in an asymmetrical roughened flume. Vertical distributions and contour plots of longitudinal velocity are presented in Figures 6 and 7. In Figure 6, the blue line represents the water surface. Figure 7 presents velocity data for Q = 0.0556 m3/s at x = 1.9 m towards the upstream end of the sidewall rib.

For one discharge (Q = 0.0556 m^3/s), longitudinal velocity measurements at three longitudinal locations showed a quasi-uniform flow field at the upstream end of the flume, i.e. at 0.9 m from the start of the rib, where the boundary layer regions were not fully developed (Fig. 7). Further downstream in the ribbed channel, the velocity distributions were fully-developed. The maximum velocities were closer to the smooth left sidewall

and low velocity regions were observed in the cavity beneath the rib. The longitudinal velocities in the cavity increased by about 20-25% from the upstream end to the downstream end of the rib, in line with the increase in cross-sectional averaged velocity V_{mean} from x = 1.9 m to 11.9 m. Some complex velocity pattern was observed near the edges of the rib, evidences of strong secondary currents.

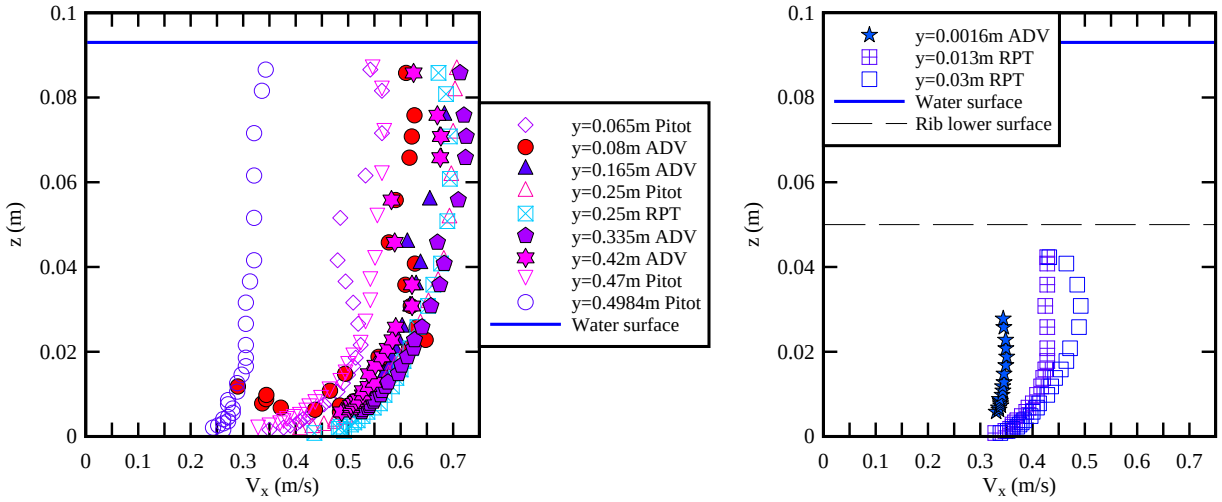

Figure 6. Vertical profiles of longitudinal velocity component V_x (m/s) in the sidewall ribbed channel at for Q = 0.0261 m^3/s at x = 8 m. Right: profiles beneath the square rib (0 < y < 0.05 m); Left: other profiles (0.05 m < y < 0.5 m).

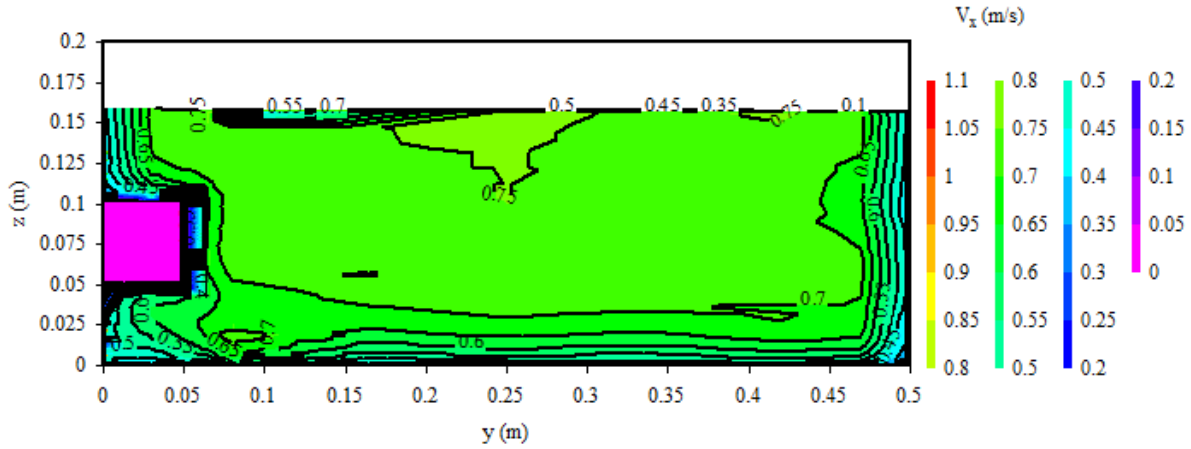

Figure 7. Contour plots for longitudinal velocity V_x (m/s) in the ribbed channel for Q = 0.0556 m^3/s at x = 1.9 m, looking upstream. Note the square rib on the left of the graph.

Boundary shear stress measurements were performed along the wetted perimeter in the ribbed channel. Figure 8 presents typical transverse distributions of dimensionless (skin friction) boundary shear stress along the wetted perimeter at three longitudinal locations, where f_{skin} is dimensionless skin friction shear stress and f is the dimensionless total boundary shear stress (Table 1). Figure 8a shows the definition of the wetted perimeter coordinate y", with the origin being the bottom right corner of the flume. In Figure 8b, the vertical black lines represent physical corners, internal or external. The experimental data showed the non-uniform distribution of boundary shear stress along the wetted perimeter. The skin friction boundary shear stress was not symmetrically distributed about the channel centreline. Large boundary shear stresses were recorded along the faces of the sidewall rib, with maximum shear stresses typically observed on the vertical side of the rib and external corners which might be related to local fluid acceleration and streamwise vorticity. Such large skin friction shear stresses might suggest a region of strong interactions between the main flow, secondary currents and cavity recirculation, in a manner similar to observations on heterogeneous transverse roughness (Tominaga and Nezu 1991). Along the channel bottom, the skin friction data presented a transverse shape

with two dips, observed about y/B = 0.4 and 0.85. The bottom profile hinted the existence of two large longitudinal vortical structures in the main flow region, plus one longitudinal structure in the cavity beneath the rib.

In the ribbed channel, the skin friction boundary shear stress was less than the total boundary shear stress: i.e., $f_{skin}/f < 1$ (Fig. 8b). The finding implies that the total flow resistance of sidewall ribbed channel was a combination of skin friction and form drag induced by secondary motion and turbulent dissipation around the rib.

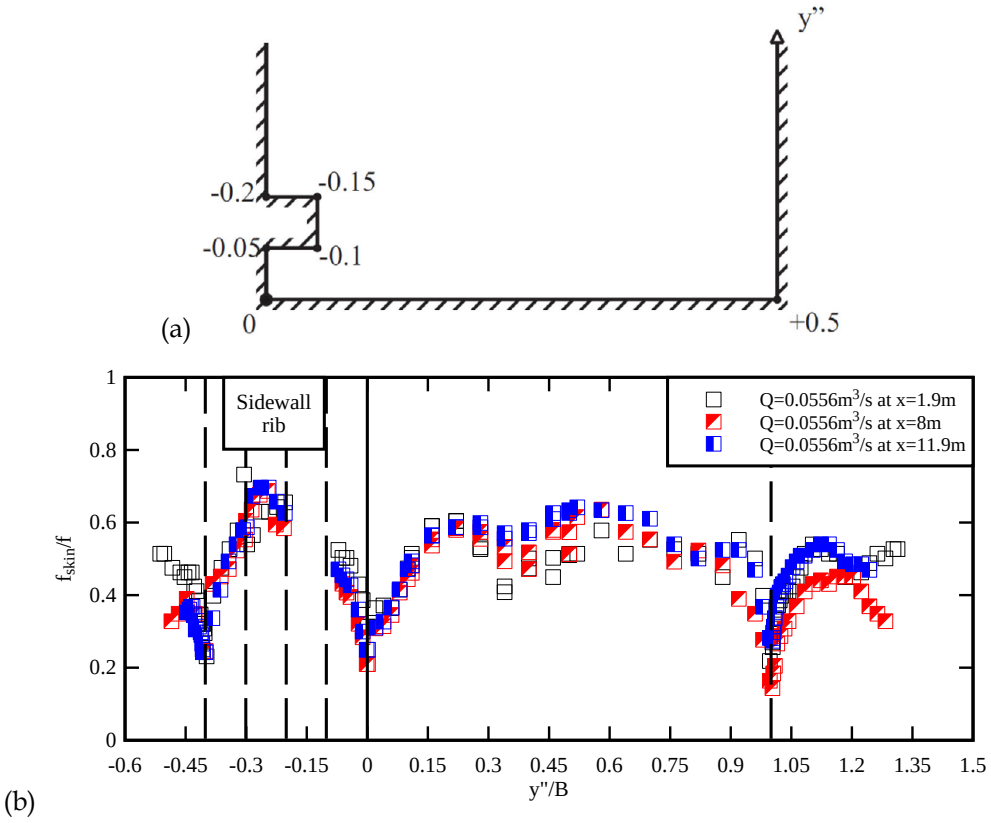

Figure 8. Transverse distributions of dimensionless boundary shear stress along the wetted perimeter of the sidewall ribbed channel. (a) Definition of wetted perimeter coordinate y" along the ribbed channel section, looking upstream, with the units in metres. (b) Dimensionless boundary shear stress f_{skin}/f for Q = 0.0556 m^3/s x = 1.9 m, 8 m and 11.9 m, with the vertical lines indicating inner and outer corners.

5 DISCUSSION

Both flow visualisations and flow resistance data showed three-dimensional flow patterns and energy dissipation associated with the rib presence. In average, the flow resistance was larger than basic skin friction, implying a 30% reduction in the channel discharge capacity for a given afflux, consistent with previous studies (Kennedy and Fulton 1965). Complicated secondary currents of Prandtl's second kind developed, in particular next to the square rib, linked to low-velocity and high-turbulence, contributing to strong turbulent dissipation. A feature was the provision of a small well-marked highly-turbulence low-velocity zone (LVZ) beneath the sidewall rib, for all tested flow conditions. The detailed velocity data were used to quantify the relative size of low velocity zones, associated with each flow rate. Figure 9 presents the results, as the fraction of wetted cross-sectional area where the ratio of longitudinal velocity to mean velocity was: $V_x/V_{mean} < 0.3$, 0.5, 0.75 and 1. Overall, the percentage of flow area where V_x/V_{mean} was less than 0.3 was less than 3%. The relative flow area where $V_x/V_{mean} < 0.75$ ranged from 16% to 25%. The results suggested drastic changes in low velocity zone (LVZ) sizes depending upon the definition of LVZ and the velocity target. The present data were compared to earlier studies in similar-size rectangular channel (Wang et al. 2018, Cabonce et al. 2019) (Fig. 9). The ribbed channel configuration provided substantially smaller low velocity zones, for the same flow rates, than the asymetrical roughened channel configuration (Fig. 9. black symbols). Further comparison with smooth flume data showed comparable LVZ sizes in smooth rectangular flume and ribbed channel.

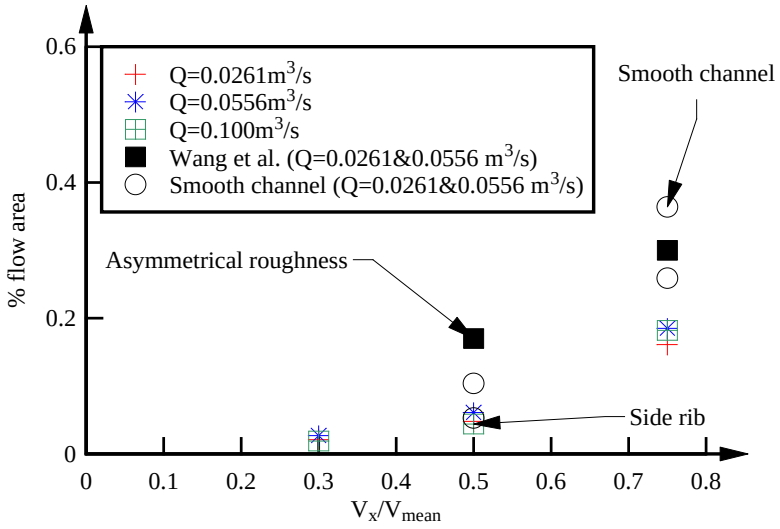

Figure 9. Fractions of low velocity regions where V_x/V_{mean} is less than a set value, for different discharges in the sidewall ribbed channel at x = 8 m. Comparison with the asymmetrical roughened channel data of Wang et al. (2018) (black symbols) and smooth channel data (Cabonce et al. 2019).

The longitudinal sidewall rib configuration may be applied to hydraulic structure designs, e.g. for the growth of biofilms, enhancement of contaminant mixing in streams, or the upstream passage of fish in culverts and fish passes. Practically, a number of technical challenges are directly linked to the design, manufacturing and installation of the rib, as well its operation. The preferred manufacturing of a ribbed channel would be in factory, to ensure that the rib position and alignment are within specifications. In the present study, the rib was installed with an error on the longitudinal rib height less than 1 mm over the entire 12 m. In-situ installation of the rib would not meet the same standards, leading to a substantially different flow field, with adverse impact on the channel operation and function. The current study was conducted with a sharp-edge rib, because sharp edges and corners constitute well-known hydrodynamic discontinuity, conducive of strong secondary current. Any rounding of the corner edges or corner would modify significantly the whole turbulent flow field. During operation, the 0.05×0.05 m^2 square flow cavity beneath the rib would only be suitable to small-body fish, shorter than 0.05 m, and there are high risks of blockage by sediments and debris. The accumulation of solid particles beneath the rib could lead to a partial or complete blockage of the low velocity region, because the cavity flow is slow and below current guidelines for self-cleaning (QUDM 2013). Larger debris, including rocks, branches, trees, could also become jammed beneath the rib, obstructing the square cavity and reducing further the channel discharge capacity.

Simply, the application of sidewall rib to hydraulic structures must be considered with uttermost care. A number of practical considerations showed major technical issues during design, manufacturing, installation and operation. In many instances, alternative designs should be preferred and implemented, especially at hydraulic structures to assist fish passage, e.g. asymmetrically roughened culvert barrel and barrel equipped with small closely-spaced triangular corner baffles, although the optimum type of boundary treatment might be closely linked to the targeted fish species.

6 CONCLUSIONS

Channels with streamwise ribs have been studied for decades in chemical engineering, environmental and sanitary engineering, aeronautics, astronautics, biology and geology. A detailed physical study was conducted in an asymmetrical rectangular channel equipped with a sidewall streamwise rib. Both flow visualisations and flow resistance data showed three-dimensional flow patterns and energy dissipation associated with the rib presence. A feature of the channel design was the provision of a small highly-turbulent low-velocity zone beneath the sidewall rib, for all tested flow conditions. Free-surface, velocity and boundary shear stress measurements showed intense secondary currents of Prandtl's second kind, induced by the presence of the inner and outer corners of the rib.

Recently a group of biologists (Watson et al. 2018) claimed "*novel remediation strategies to improve fish passage through culverts*" in the form of "*novel beam designs*". It is demonstrated that the longitudinal beam

design is not new, having been used in sanitary engineering, water treatment and heat-and-mass transfer applications for more than a century, including in biology. The results of the current hydrodynamic study showed un-equivocally that the flow in an asymmetrical ribbed channel is extremely complicated, and that the design presents a number of manufacturing, installation and operational flaws, including very-high risks of blockage by sediments and debris. In many instances, alternative designs should be preferred to assist fish passage at hydraulic structures, including culverts and fishways.

ACKNOWLEDGEMENTS

The authors thank Dr John Macintosh (Water Solutions, Australia), Professor Oscar Castro-Orgaz (University of Cordoba, Spain), and Professor Benoit Cushman-Roisin (Dartmouth College, USA) for their very valuable comments. They thank further Professor Donald Knight (University of Birmingham, UK) and Professor Colin Apelt (The University of Queensland, Australia) for helpful advice. The authors acknowledge the assistance of Ms Matilda Meppem during some experiment. They acknowledge the technical assistance of Jason Van Der Gevel and Stewart Matthews (The University of Queensland). The financial support through the Australian Research Council (Grant LP140100225) is acknowledged.

Hubert Chanson has competing interest and conflict of interest with Craig E. Franklin.

REFERENCES

Bushnell,.D.M., and McGinley, C.B. (1989). Turbulence control in wall flows. *Annual Review of Fluid Mechanics*, Vol. 21, pp. 1-20.

Cabonce, J., Fernando, R., Wang, H., and Chanson, H. (2017). Using Triangular Baffles to Facilitate Upstream Fish Passage in Box Culverts: Physical Modelling. *Hydraulic Model Report No. CH107/17*, School of Civil Engineering, The University of Queensland, Brisbane, Australia, 130 pages.

Cabonce, J., Fernando, R., Wang, H., and Chanson, H. (2019). Using Small Triangular Baffles to Facilitate Upstream Fish Passage in Standard Box Culverts. *Environmental Fluid Mechanics*, Vol. 19, No. 1, pp. 157–179 (DOI: 10.1007/s10652-018-9604-x).

Carling, P.A., Williams, J.J., Croudace, I.W., and Amos, C.L. (2009). Formation of mud ridge and runnels in the intertidal zone of the Severn Estuary, UK. *Continental Shelf Research*, Vol. 29, pp. 1913-1926.

Chang, S.W., Lin, C.C., and Liou, J.S. (2008). Heat Transfer in a Reciprocating Curved Square Duct Fitted with Longitudinal Ribs. *International Journal of Thermal Science*, Vol. 47, pp. 52-67.

Chanson, H. (2000). Boundary Shear Stress Measurements in Undular Flows: Application to Standing Wave Bed Forms. *Water Resources Research*, Vol. 36, No. 10, pp. 3063-3076 (DOI: 10.1029/2000WR900154).

Chanson, H. (2004). *The Hydraulics of Open Channel Flow: An Introduction*. Butterworth-Heinemann, 2nd edition, Oxford, UK, 630 pages.

Chanson, H., Trevethan, M., and Aoki, S. (2008). Acoustic Doppler Velocimetry (ADV) in Small Estuary: Field Experience and Signal Post-Processing. *Flow Measurement and Instrumentation*, Vol. 19, No. 5, pp. 307-313 (DOI: 10.1016/j.flowmeasinst.2008.03.003),

Degremont (1979). *Water Treatment Handbook*. Halsted Press Book, John Wiley & Sons, 5th edition, New York, USA.

FNDAE (1988). Les Bassins d'Orage sur les Réseaux d'Assinissement. *Documentation technique No. 6*, Fonds National pour le Développement des Adducations d'eau, Ministère de l'Agriculture, Paris, France, 61 pages (in French).

Goring, D. and Nikora, V.I. (2002). Despiking Acoustic Doppler Velocimeter Data. *Journal of Hydraulic Engineering*, ASCE, Vol. 128, No. 1, pp. 117-126. Discussion: Vol. 129, No. 6, pp. 484-489.

Henderson, F.M. (1966). *Open Channel Flow*. MacMillan Company, New York, USA.

Itoh, M., Tamano, S., Igushi, H., Yokota, K., Akino, N., Hino, R., and Kubo, S. (2006). Turbulent drag reduction by the seal fur surface. *Physics of Fluids*, Vol. 18, Paper 065102, 9 pages.

Kennedy, R.J., and Fulton, J.F. (1961) The Effect of Secondary Currents Upon the Capacity of a Straight Open Channel. Transactions, *Engrg. Inst. of Canada*, Vol. 5, No. 1, pp. 12-18.

Knight, D.W., and Macdonald, J.A. (1979). Hydraulic Resistance of Artificial Strip Roughness. *Jl of Hyd. Div.*, ASCE, Vol. 105, No. HY6, June, pp. 675-690.

Macintosh, J.C. (1990). Hydraulic Characteristics in Channels of Complex Cross-Section. *Ph.D. thesis*, University of Queensland, Dept of Civil Engineering, Australia, November, 487 pages.

Morris, H.M. (1955). A New Concept of Flow in Rough Conduits. *Transactions*, ASCE, Vol. 120, pp. 373-410.

Naik, S., Probert, S.D., and Bryden, I.G. (1999). Heat Transfer Characteristics of Shrouded Longitudinal Ribs in Turbulent Forced Convection. *International Journal of Heat and Mass Transfer*, Vol. 20, pp. 374-384.

Nezu, I., and Nakagawa, H. (1984). Cellular Secondary Currents in Straight Conduits. *Journal of Hydraulic Engineering*, ASCE, Vol. 110, No. 2, pp. 173-193.

Nitschke, P. (1983). Experimentelle Undersuchung der turbulenten Stroemung in glatten und laengsgerillten Rohren. *Max-Planck Institue fur Stromungsforschung*, Goettingen, West Germany (in German).

Patel, V.C. (1965). Calibration of the Preston Tube and Limitations on its use in Pressure Gradients. *Journal of Fluid Mechanics*, Vol. 23, Part 1, Sept., pp. 185-208.

QUDM (2013). *Queensland Urban Drainage Manual*. Queensland Department of Energy and Water Supply, Brisbane, Australia, Third edition, 459 pages.

Randtke, S.J., and Horsley, M.B. (2012). *Water Treatment Plant Design*. McGraw-Hill, American Water Works Association and American Society of Civil Engineers, 5th edition.

Roo, J.T. (1965). Horizontal Filter Structure. *US Patent 3,216,576*, Publication US3216576A, 4 pp & 4 plates.

Sanchez, P.X., Leng, X., and Chanson, H. (2018). Fluid Dynamics and Secondary Currents in an Asymmetrical Rectangular Canal with Sidewall Streamwise Rib. *Hydraulic Model Report No. CH113/18*, School of Civil Engineering, The University of Queensland, Brisbane, Australia, 158 pages.

Stamou, A. (2008). Improving the hydraulic efficiency of water process tanks using CFD models. *Chemical Engineering and Processing*, Vol. 47, pp. 1179-1189.

Tanaka, K.L. (1999). Debris-flow origin for the Simud/Tiu deposit on Mars. *Journal of Geophysical Research-Planets*, Vol. 104, No. E4, pp. 8637-8652 (DOI: 10.1029/98JE02552).

Tominaga, A., and Nezu, I. (1991). Turbulent Structure of Shear Flow with Spanwise Roughness Heterogeneity. *Proc. International Symposium on Environmental Hydraulics*, Hong Kong, 16-18 Dec., Balkema Publ., Rotterdam, pp. 415-420/

Wang, H., Uys, W., and Chanson, H. (2018). Alternative Mitigation Measures for Fish Passage in Standard Box Culverts: Physical Modelling. *Journal of Hydro-environment Research*, IAHR, Vol. 19, pp. 214-223 (DOI: 10.1016/j.jher.2017.03.001).

Watson, J., Goodrich, H., Cramp, R., Gordos, M., and Franklin, C.E. (2018).Utilising the Boundary Layer to Help restore the Connectivity of Fish Habitat and Population. *Ecol. Eng.*, Vol. 122, pp. 286-294.